

## Combined therapies of antithrombotics and antioxidants delay *in silico* brain tumor progression

ALICIA MARTÍNEZ-GONZÁLEZ\*

*Departamento de Matemáticas, Universidad de Castilla-La Mancha  
ETSI Industriales, Avda. Camilo José Cela 3, 13071 Ciudad Real, Spain.*

\*Corresponding author: alicia.martinez@uclm.es

MARIO DURÁN-PRADO

*Dpto. de Ciencias Médicas, Facultad de Medicina, Universidad de Castilla-La Mancha,  
13071 Ciudad Real, Spain.*

GABRIEL F. CALVO

*Departamento de Matemáticas, Universidad de Castilla-La Mancha  
ETSI Caminos, Canales y Puertos, Avda. Camilo José Cela 3, 13071 Ciudad Real, Spain.*

FRANCISCO J. ALCAÍN

*Dpto. de Ciencias Médicas, Facultad de Medicina, Universidad de Castilla-La Mancha,  
13071 Ciudad Real, Spain.*

LUIS A. PÉREZ-ROMASANTA

*Servicio de Oncología Radioterápica, Hospital General Universitario de Salamanca, Spain*

VÍCTOR M. PÉREZ-GARCÍA

*Departamento de Matemáticas, Universidad de Castilla-La Mancha  
ETSI Industriales, Avda. Camilo José Cela 3, 13071 Ciudad Real, Spain.*

[Received on XXXXX]

Glioblastoma multiforme, the most frequent type of primary brain tumor, is a rapidly evolving and spatially heterogeneous high-grade astrocytoma that presents areas of necrosis, hypercellularity and microvascular hyperplasia. The aberrant vasculature leads to hypoxic areas and results in an increase of the oxidative stress selecting for more invasive tumor cell phenotypes. In our study we assay *in silico* different therapeutic approaches which combine antithrombotics, antioxidants and standard radiotherapy. To do so, we have developed a biocomputational model of glioblastoma multiforme that incorporates the spatio-temporal interplay among two glioma cell phenotypes corresponding to oxygenated and hypoxic cells, a necrotic core and the local vasculature whose response evolves with tumor progression. Our numerical simulations predict that suitable combinations of antithrombotics and antioxidants may diminish, in a synergetic way, oxidative stress and the subsequent hypoxic response. This novel therapeutical strategy, with potentially low or no toxicity, might reduce tumor invasion and further sensitize glioblastoma multiforme to conventional radiotherapy or other cytotoxic agents, hopefully increasing median patient overall survival time.

**Keywords:** Glioblastoma multiforme, antithrombotic, radiotherapy, antioxidants, combined therapies

## 1. Introduction

Glioblastoma Multiforme (GBM), a World Health Organization (WHO) grade IV astrocytic glioma, is the most aggressive and frequent primary brain tumor (Louis et al., 2007). GBM may develop (spanning from 1 year to more than 10 years) from lower-grade astrocytomas (WHO grade II) or anaplastic astrocytomas (WHO grade III), but more frequently, it manifests *de novo*. The median overall survival ranges from 12 to 15 months after diagnosis despite using the current standard care. It includes maximal safe resection followed by radiotherapy in combination with the chemotherapeutic (alkylating) agent temozolomide (Van Meir et al., 2010). After treatment, relapse occurs typically within a few months due to the GBM radio and chemoresistance and its remarkable infiltrative nature.

At the tissue level, the presence of necrosis and microvascular hyperplasia is characteristic of GBM, in contrast to lower-grade gliomas where peritumoral vascular damage is infrequent or absent. Histological samples of GBM frequently show thrombosed vessels within necrotic cores. Tumor cells actively migrate away from oxygen-deficient (hypoxic) regions, originated after vascular injury. They form hypercellular regions that surround the necrotic cores (Rong et al., 2006).

At the molecular level, adaptation of tumor cell subpopulations to strong spatio-temporal variations of oxygen availability is mediated by the hypoxia-inducible factor (HIF-1). This complex activates the transcription of hundreds of genes that play key roles, among others, in cell death avoidance, genetic instability, vascularization, glucose metabolism, pH regulation, immune evasion and invasion (Kelly et al., 2008; Semenza, 2012). Under acute hypoxia, tumor cells will tend to cease or reduce their proliferation rate as a means to decrease oxygen consumption. This mechanism relies primarily on the subunit HIF-1 $\alpha$  of the heterodimer HIF-1, which arrests DNA replication in the presence of oxygen stress (Hubbi et al., 2013). Moreover, the levels of free radicals increase during cycles of hypoxia and there is evidence that they are also molecular switches influencing the stabilization of HIF-1 $\alpha$  (Wilson and Hay, 2011).

In contrast to normal cells, the survival of GBM cells is favored by an increase in free radicals since the oxidative stress forces the cells to produce antioxidant enzymes such as catalase and superoxide dismutase to control the exacerbated level of free radicals (Kovacic and Osuna, 2001; Schumacker, 2006). The increase in these antioxidant enzymes strongly interferes with the action of radio/chemotherapy, that kill tumor cells by inducing an increase in free radicals (Tennant et al., 2010). In addition, free radicals inactivate the tumor suppressor protein p53, enabling tumor cells to escape apoptosis (Cobbs et al., 2003). Thus, disrupting this signaling process in tumors, may be expected to promote hypoxia-induced death (Joiner et al., 2009) and to restore redox homeostasis, turning off the hypoxic response.

Many evidences indicate that the invasive ability of GBM and its resistance to chemo and radiotherapy is mostly due to phenotypic changes that are intimately linked to the presence of hypoxia, initiated by oxygen deprivation after a vaso-occlusion event. Under these conditions, the levels of HIF-1 $\alpha$  increase driving the expression of many pro-angiogenic factors such as the Vascular Endothelial Growth Factor (VEGF). The accumulation of VEGF promotes an aberrant neovascularization (Semenza, 2009) composed of a high density of non functional microvessels which are leaky and devoid of pericytes. This structure allows the contact between blood and tumor cells and initiates the coagulation cascade and the formation of thrombi, a major cause of patient death (Jenkins et al., 2010; Young et al., 2012). Furthermore, the transmembrane protein tissue factor (TF) not only activates the extrinsic pro-coagulant pathway but also contributes to GBM cell invasion and neovascularization (Harter et al., 2013). In general, thromboembolism, i.e. vaso-occlusion events of large vessels, is recognized as a major complication of cancer and a common cause of death in cancer patients. There is strong evidence linking venous thromboembolism (VTE) and malignancy (Khorana and Francis, 2008; Green and Kwaan, 2009).

Thromboembolic complications include a broad spectrum of clinical problems, a fact that has led to the use of different ways of thromboprophylaxis (Khorana and Francis, 2008; Green and Kwaan, 2009) for cancer patients. Bastida et al. (1984) proved that glioma cell lines secrete pro-thrombotic factors, and in fact, glioma patients have a high incidence of VTE, with several studies suggesting that 25%-30% of these patients suffer thromboembolic events (Streiff et al., 2004; Simanek et al., 2007).

It is also known that the more tumoral tissue is removed during surgery of high-grade gliomas the less-likely are the patients to die from VTE (Brose and Lee, 2008; Simanek et al., 2007). Thus, all this body of evidence has led to the consideration of thromboprophylaxis using anticoagulants, such as for instance low molecular weight heparine (LMWH), for glioma patients, specially in those with a high potential risk of developing VTE (Hamilton et al., 1994; Batchelor and Byrne, 2006; Jenkins et al., 2010; Khorana and Francis, 2008).

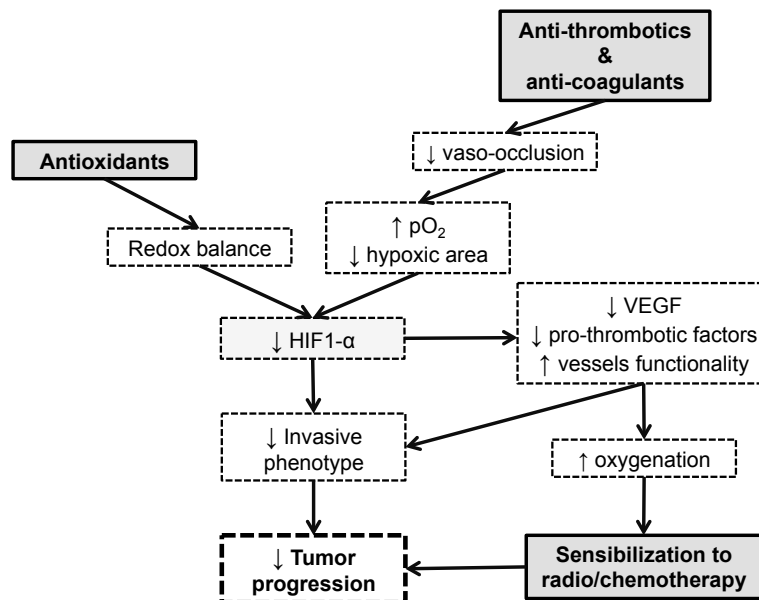
In addition to their potential use to diminish the risk of VTE, LMWH exerts a direct effect on tumor cells and tumor stroma, as it can directly kill cancer cells and also inhibit the neovascularization process, which downregulates cell invasion (Santos et al., 2010; Svensson et al., 2011; Green and Kwaan, 2009). In this context, there have been a limited number of small-scale clinical studies evaluating the safety of antithrombotic therapy in GBM patients with a VTE risk supporting the safety of the approach (Schneider et al., 2010). However, no extra benefits beyond the substantial reduction in the VTE risk have been proven yet.

In our previous study (Martínez-González et al., 2012), we developed a minimal mathematical model of GBM progression incorporating the evolution of different tumor cell subpopulations and chemicals in the tumor microenvironment. The implications of that work are that antithrombotics would have a restrain effect on tumor progression, thus allowing a better local control of the tumor. However the potential gain achieved by the use of antithrombotics alone is modest. In this paper we will discuss a way to potentially obtain a much more substantial tumor control by targetting simultaneously the vessel occlusion events and the accumulation of hypoxia inducible factors.

Thus, in this paper we study *in silico* a more elaborated system, including two different cell phenotypes, the oxygen concentration in the brain tissue and a dynamic vasculature to assess the potential effect of combined therapies targetting simultaneously the vessel-occlusion events and the “normalization” therapy (antioxidation) together with standard radiotherapy as an example of cytotoxic therapy.

Our conceptual framework is summarized in Fig. 1. Vascular regularizing therapies and antioxidants follow different pathways aimed at reducing tumor hypoxia by means of directly impacting on HIF-1 $\alpha$  levels. This effect would decrease oxidative stress and the subsequent hypoxic response. To achieve this goal, antioxidants act on the oxidation balance whereas antithrombotics reduce vaso-occlusions and hypoxic areas. The overall effect is an increment in oxygenation. Both therapies should ameliorate vessel functionality by reducing pro-thrombotic and angiogenic factors. In addition, the higher oxygen levels and decreased oxidative stress may provide the extra benefit of a sensitization to radio and chemotherapy, that might result in a synergistic response to the treatment.

Our plan in this paper is as follows. First, in Sec. 2 we present the basic model equations describing tumor progression in detail and discuss the assumptions behind them. Next, in Sec. 3 we discuss how to incorporate the different therapies into the model. Parameter estimation is addressed in Sec. 4. Once the model is set up and realistic parameter ranges identified we move on to studying the dynamics; the main results being outlined in Sec. 5. Finally, in Sec. 6 we discuss the implications of our findings and summarize our conclusions.



+

## 2.1 Cell phenotypes

Following these biological facts we will assume in our model that the heterogeneous oxygen distribution is the driving force that triggers phenotypic changes of tumor cells as shown schematically in Fig. 2. Thus, the local oxygen concentration will be considered to have a major influence on the cell phenotype expression. It will be assumed to induce spatio-temporal variations of phenotypic expressions via the HIF-1 $\alpha$  activation/deactivation pathways. Therefore, will focus ourselves only on two dominant tumor cell phenotypes. A first phenotype with a spatio-temporal density described by a non-negative function  $C_n(x, t) : \mathbb{R}^2 \rightarrow \mathbb{R}_0^+$  corresponds to more proliferative tumor cells. A second phenotype

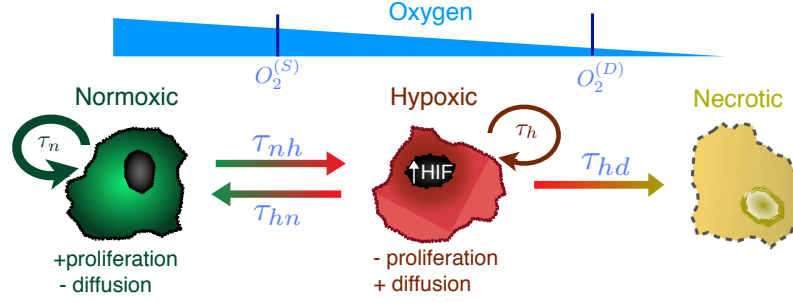


FIG. 2. **Oxygen pressure influences the phenotype of a tumor cell.** Depending on the oxygen pressures various switching mechanisms arise coupling the populations: Normoxic to hypoxic  $S_{nh}$  for oxygen concentrations  $O_2^{(S)}$  with characteristic time  $\tau_{nh}$ ; hypoxic to normoxic  $S_{hn}$  above  $O_2^{(S)}$  with characteristic time  $\tau_{hn}$  and hypoxic to necrotic  $S_{hd}$  for pressures below  $O_2^{(D)}$  with characteristic time  $\tau_{hd}$ . High oxygen pressures favor the existence of less mobile phenotypes with shorter doubling times  $\tau_n$ . On the contrary, cells respond to low oxygen pressures by expressing more motile phenotypes with larger doubling times  $\tau_h$  (Brat et al., 2004).

will be described by (a nonnegative) function  $C_h(x, t) : \mathbb{R}^2 \rightarrow \mathbb{R}_0^+$  accounting for tumor cells which are more mobile and resistant to therapies. Both phenotypes have been described to have a major role in GBM progression (DeBerardinis et al., 2007; Giese et al., 2003; Keunen et al., 2011; Onishi et al., 2011). For convenience, we will refer to them somewhat imprecisely as “normoxic” and “hypoxic” phenotypes since they correspond to the limit behavior of the tumor cell density after either very long oxygenation periods ( $C_n(x, t)$ ) or persistent oxygen deprivation periods ( $C_h(x, t)$ ).

The equations governing the interplay between the dominant phenotypes are

$$\frac{\partial C_n}{\partial t} = D_n \nabla^2 C_n + \frac{C_n}{\tau_n} \left( 1 - \frac{C_n + C_h + C_d}{C^{(M)}} \right) + \frac{S_{hn}}{\tau_{hn}} C_h - \frac{S_{nh}}{\tau_{nh}} C_n, \quad (2.1a)$$

$$\frac{\partial C_h}{\partial t} = D_h \nabla^2 C_h + \frac{C_h}{\tau_h} \left( 1 - \frac{C_n + C_h + C_d}{C^{(M)}} \right) - \frac{S_{hn}}{\tau_{hn}} C_h + \frac{S_{nh}}{\tau_{nh}} C_n - \frac{S_{hd}}{\tau_{hd}} C_h. \quad (2.1b)$$

The first right-hand-side terms in Eqs. (2.1a) and (2.1b) account for cellular motility. Since the hypoxic phenotype is more migratory than the normoxic one (Berens and Giese, 1999; Giese et al., 2003; Bristow and Hill, 2008; Gorin et al., 2004), the hypoxic cell diffusion coefficient  $D_h$  should be chosen to be larger than the normoxic one  $D_n$ . This is a key assumption of our model whose implications will be elucidated in detail.

The second terms in Eqs. (2.1a) and (2.1b) are classical logistic growth terms for the tumor cell populations with proliferation times  $\tau_n$  and  $\tau_h$ , respectively, and a maximum cell density  $C^{(M)}$  that the brain tissue can accommodate. The migration-proliferation dichotomy suggests that  $\tau_n < \tau_h$ ; this is also supported by the observation that hypoxic cells reduce their proliferation rate by arresting DNA replication (Hubbi et al., 2013). Since growth is assumed to be space-limited we incorporate also the necrotic tissue density  $C_d(x, t)$  into the saturation terms (see below).

The third and fourth terms in Eqs. (2.1a) and (2.1b) represent the phenotypic switch under different oxygenations. The *switch* functions  $S_{nh}$ ,  $S_{hn}$  depend on the oxygen pressure. Under low oxygen conditions ( $O_2^{(S)} < 7$  mmHg), normoxic cells change their phenotype to the hypoxic one, whereas above  $O_2^{(S)}$  hypoxic cells recover their oxic phenotype.  $\tau_{nh}$  and  $\tau_{hn}$  denote the characteristic switching times

of these processes. Usually  $\tau_{nh}$  is much shorter than  $\tau_{hn}$  since cells incorporate mechanisms to respond almost instantaneously to the absence of oxygen. However the reverse process is not so fast, specially in cells that have already suffered several oxygen deprivation episodes (Hsieh, 2010).

To close the model we have to incorporate an equation for the necrotic tissue density  $C_d(x, t)$

$$\frac{\partial C_d}{\partial t} = \frac{S_{hd}}{\tau_{hd}} C_h. \quad (2.1c)$$

Hypoxic cells (2.1b) feed the necrotic tissue in Eq. (2.1c) under persistent anoxic ( $O_2^{(D)} < 0.7$  mmHg) conditions. This is accounted for by the switch function  $S_{hd}$  and a rate  $1/\tau_{hd}$ . The explicit form of the switch functions will be taken to be (Martínez-González *et al.*, 2012)

$$S_{nh}(O_2) = \frac{1}{2} \left[ 1 - \tanh \left( \frac{O_2 - O_2^{(S)}}{\Delta O_2} \right) \right], \quad (2.2a)$$

$$S_{hn}(O_2) = \frac{1}{2} \left[ 1 + \tanh \left( \frac{O_2 - O_2^{(S)}}{\Delta O_2} \right) \right], \quad (2.2b)$$

$$S_{hd}(O_2) = \frac{1}{2} \left[ 1 - \tanh \left( \frac{O_2 - O_2^{(D)}}{\Delta O_2} \right) \right] \quad (2.2c)$$

were the three step-like switch functions  $S_{nh}$ ,  $S_{hn}$  and  $S_{hd} \in [0, 1]$  and the parameter  $\Delta O_2$  described the characteristic range of oxygen variations where the transitions occur.

## 2.2 Modelling oxygen distribution through the tissue

To simplify the analysis, yet retaining the basic interplay of the key underlying biological processes in GBM, we will stick to a one dimensional geometry with the oxygen flow coming from a network (1D lattice) of vessels. In the brain, spatio-temporal inhomogeneities arise in the parameter values (e.g. different propagation speeds in white and gray matter which also vary in time as the tumor progresses) and anisotropies (e.g. on the diffusion tensor with preferential propagation directions along white matter tracts (Painter and Hillen, 2013)). However, those complexities would add on top of the phenomena to be described in this paper. Thus, in what follows, we will focus our study on a representative spatial section which will provide key spatial and time metrics enabling us to incorporate, at a later stage, the action of various therapeutic modalities.

The spatio-temporal evolution of oxygen  $O_2(x, t)$  is similar to the one chosen in Martínez-González *et al.* (2012), although now oxygen sources are located on the blood vessels, and is governed by

$$\frac{\partial O_2}{\partial t} = D_{O_2} \nabla^2 O_2 - \frac{\alpha_n C_n + \alpha_h C_h}{O_2^{(T)} + O_2} O_2 + J \chi^C (\chi^F O_2^{v_i} - O_2). \quad (2.3)$$

The first term in the right-hand-side of Eq. (2.3), accounts for oxygen diffusion in the brain tissue and assumes an homogenous and isotropic diffusion coefficient  $D_{O_2}$ . The second term models the oxygen consumption by both normoxic and hypoxic cells at rates  $\alpha_n$  and  $\alpha_h$ , respectively. The saturation Michaelis-Menten constant  $O_2^{(T)}$  corresponds to the oxygen pressure level at which the reaction rate is halved. The third term describes the oxygen flow from the vessels to the tissue. The oxygen pressure in the  $i^{th}$  blood vessel will be denoted as  $O_2^{v_i}(t)$ . The multiplicative function  $J(x)$  in Eq. (2.3) accounts

for the spatial distribution of the oxygen supply and depends on the blood vessels positions  $p_i$  and their sizes  $v_i$ . Here,  $J$  will be taken to be a combination of Gaussian functions of the form

$$J(x) = J_{O_2} \sum_{i=1}^N e^{-(x-p_i)^2/v_i^2}, \quad (2.4)$$

with  $J_{O_2} = 10^{-6} s^{-1}$  as the estimation for the oxygen exchange coefficient which is considered to be constant in time and the same for all of the vessels. The positions  $p_i$  of the vessels will be considered to be equidistant, with separations of  $300 \mu m$ . The vessel widths  $v_i$  (being capillaries), will be taken to be  $30 \mu m$  in diameter. Since oxygen diffuses along and through the vasculature it is reasonable to think that vessels of similar size will have similar nutrient concentrations. Therefore,  $O_2^{v_i}$  is considered to be constant along time for all  $i$ . Furthermore,  $\chi^C$  and  $\chi^F$  in Eq. (2.3) are factors accounting for the chronic and fluctuating hypoxia induced by the tumor and will be explained in depth in Section 2.3.

Oxygen diffuses successively through the intracellular fluid, cell membranes and cytoplasm which have abrupt spatial variations. However, previous works (Pogue et al., 2001; Daçu et al., 2003; Powathil et al., 2012) have proved that using an average diffusion coefficient for oxygen as in Ec. (2.3) provides a good approximation to the diffusion process.

Given that mean oxygen pressure in arterial blood is around 95 mmHg (Kimura et al., 1996) and venous values are around 30-40 mmHg, we will employ for the oxygen pressure within the capillaries a constant value  $O_2^{v_i} = 80$  mmHg.

### 2.3 Vasculature and coagulation

The sources of nutrients and oxygen in the brain are the blood vessels (capillaries in here). We will also assume that oxygen concentration in the capillary network does not follow the variations induced by the cardiac pumping in the major blood vessels (Daçu et al., 2003), because of the fast time scale of those variations.

Thrombi formation leading to the developing of pseudopalisading structures (Brat et al., 2004; Rong et al., 2006) may be in part connected with the vascular remodeling induced by tumor cells. The pro-angiogenic stimuli give rise to hyperplasia in the endothelial cells which lose cell to cell unions causing vascular permeability and a malfunctioning of the blood-brain barrier (BBB). The generated orifices allow the blood to be in contact with the tumor cells. It results in plasma coagulation factors in direct connection with the tumor tissue. As a consequence, fibrin coagulates and platelets aggregate. The tumor secretes TF that activate the so-called extrinsic coagulation pathway what provides an additional source for the strong pro-thrombotic activity of GBM (Ruf et al., 2010).

We will consider that vessel functionality decreases as tumor cell density increases. Once cells accumulate around the vessels the constitutive expression of TF by cancer cells will trigger local and systemic activation of the coagulation cascade as described above.

In our approach, blood vessels will be first assumed to become semifunctional when the tumor cell density is above a certain threshold  $C^{(F)}$  implying the onset of fluctuating hypoxia. The step-like switch function  $\chi^F$  reproduces this phenomena depending on a cellular density  $C^{(F)}$  and a random dynamic noise  $z$  ( $0 < z < 1$ ) given by the equation

$$\chi^F(C_n + C_h + C_d, t^*) = 1 - z \frac{1}{2} \left[ 1 + \tanh \left( \frac{(C_n + C_h + C_d) - C^{(F)}}{\Delta c} \right) \right]. \quad (2.5a)$$

We will also assume that when the tumor cell density around the vessel grows beyond a higher threshold value  $C^{(C)}$ , the coagulation process is irreversible and chronic hypoxia sets in due to the complete lack

of oxygen flow. This process is modelled by a step-like switch function  $\chi^C$  given by

$$\chi^C(C_n + C_h + C_d, t^*) = \min \left\{ \frac{1}{2} \left[ 1 - \tanh \left( \frac{(C_n + C_h + C_d) - C^{(C)}}{\Delta c} \right) \right] : t \leq t^* \right\}. \quad (2.5b)$$

Finally, the vasculature sensitivity threshold  $\Delta c$  is estimated to be around  $0.02 C^{(M)}$  cells.

### 3. Modelling therapies

#### 3.1 Antithrombotic therapy

We will assume that low molecular weight heparine (LMWH) decreases the expression of TF and increases the vascular functionality. Thus, it prevents the formation of coagulates. This therapy will be modelled by increasing the thresholds at which the vessels become unstable from  $C^{(F)} = 0.5C^{(M)}$  to  $C^{(F)} = 0.6 - 0.8 C^{(M)}$  and from  $C^{(C)} = 0.7C^{(M)}$  to  $C^{(C)} = 0.8 - 0.99C^{(M)}$ . Although the precise values are not known and probably depend on a number of additional features, they will allow us to simulate the proof-of-principle of the antithrombotic therapy.

In addition to the prevention of VTE there are other several direct mechanisms of action of LMWH on tumor cells: direct cell killing (Santos et al., 2010), antiangiogenic effects (Svensson et al., 2011) and many others (see e.g. Green and Kwaan, 2009, Chap. 15). Since those effects are difficult to quantify we will assume in this paper that the net effect of the antithrombotic therapy is to increase the vessel functionality thresholds  $C^{(C)}$  and  $C^{(F)}$ .

In this paper we will assume that drug administration leads to a blood concentration level that is sufficient to induce the required effect and as such we will not include the details of the pharmacokinetics of the drugs. The same applied to the treatment to be described in Sec. 3.2.

#### 3.2 HIF-1 $\alpha$ stabilization treatment

When oxygen is present, HIF-1 $\alpha$  is continuously synthesized by the cell, but it is unstable and degraded with a half-life of about 2-3 minutes. However, as a consequence of the cycles of hypoxia due to the anomalous vasculature, free radicals are originated regulating and stabilizing the expression of HIF-1 $\alpha$  even when vascular functionality is restored. In fact, U87 glioma cell line shows higher HIF-1 $\alpha$  expression under cyclic than under chronic hypoxia (Hsieh, 2010). It is believed that the sequence of oxygen deprivation episodes may drive the accumulation of HIF-1 $\alpha$  in the cell nucleus. Therefore, cells need longer times to return to the normoxic phenotype state (Semenza, 2009). This HIF-1 $\alpha$  stabilization significantly increases invasiveness and secretion of angiogenic factors and drives the intrinsic and extrinsic coagulation routes.

Free radicals are usually detoxified by a complex system of proteins and antioxidant macromolecules which maintain the cell redox homeostasis. Antioxidative-based treatments, such as those with caulerpine or tempol, result in a HIF-1 $\alpha$  inhibition and consequently in an antiproliferative effect in GBM murine xenograft models (Hsieh, 2010). Thus, antioxidative-based adjuvant therapies would provide faster ways for cells to revert to their normoxic state under oxic conditions. They decrease the HIF-1 $\alpha$  accumulation and enable the recovery of the redox homeostasis. In our model, we will include the effect of the antioxidative therapy by decreasing the time of recovery of the normoxic phenotype  $\tau_{in}$  from 96 h to a smaller value in the range 8-48 h.

It is worth mentioning that based on the go or grow hypothesis, the diffusion coefficient of hypoxic cells is larger than for the normoxic cells, however, it is not known whether targeting HIF-1 $\alpha$  via an-



tioxidative therapy would induce a significant change in them. Consequently, these parameters have a 10% variability in each simulation and are constant in time along the treatments.

### 3.3 Radiotherapy

The standard radiotherapy protocol for high grade gliomas consists of a total of 60 Gy in fractions of 2 Gy given in 30 sessions from monday to friday leading to a treatment duration of 6 weeks. Treatment is usually started several (2-4) weeks after surgery.

To describe the effect of the therapy in our model, cell death induced by radiation is included in the simulations instantaneously once per day (monday to friday) during 6 weeks. We have chosen the simulations start 2 weeks after surgery, thus radiotherapy starts at week 2.

In the absence of oxygen, the unstable free radicals generated by radiation have a longer half life. Then, they can react with  $H^+$  restoring its chemically original form without the need for biological and enzymatic intervention. The overall result is that better oxygenated cells are more radiosensitive (Joiner et al., 2009). Thus we will assume the effect of radiotherapy to depend on the local oxygen concentration  $O_2(x, t)$  at the time of the therapy. Denoting by  $RT_{ox}$  the cell surviving fraction under oxic conditions and  $RT_{hyp}$  the surviving fraction under hypoxic conditions, we will employ for the total surviving fraction under a local oxygen pressure  $O_2(x, t)$ , the equation

$$S(x, t) = RT_{ox} \frac{O_2(x, t)}{O_2^{vi}} + RT_{hyp} \left( 1 - \frac{O_2(x, t)}{O_2^{vi}} \right). \quad (3.1)$$

## 4. Parameter estimation and computational details

### 4.1 Parameter estimation

We resort to available experimental values from human glioma models to obtain order-of-magnitude estimates of the intervening parameters in our equations. Typical values of the used biological parameters are shown in Table. 1 (see also further parameters details in Martínez-González et al. (2012)).

First, the maximum cell density  $C^{(M)}$  has been estimated in previous works (see e.g. Rockne et al., 2010) to be about  $10^6$  cell/cm<sup>2</sup>. Oxygen pressure threshold for hypoxic metabolism  $O_2^{(S)}$  is cell line dependent but experimental evidence supports for glioma the choice of 7 mm Hg (Vaupel, 2004). The Michaelis-Menten constant,  $O_2^{(T)}$  has to be smaller than this parameter yet larger than anoxia threshold,  $O_2^{(D)}$ , about 0.7 mm Hg (Brown et al., 2004). We have chosen it to be 2.5 mm Hg (Daču et al., 2003). The oxygen diffusion coefficient  $D_{O_2}$  is classically known to be around  $10^{-5}$  cm<sup>2</sup>/s (Daču et al., 2003) while the cell diffusion coefficients are not so readily accessible *in vivo*.

The hypoxic diffusion coefficient has been considered to be around the mean data reported in Rockne et al. (2010) and ten times larger than the normoxic one. In addition, for high-grade glioma, the largest radial velocity  $v$  ( $\approx 3$  cm/y) can be related to the hypoxic cell propagation whereas the smallest radial velocity ( $\approx 1$  cm/y) can be related to the normoxic one. For instance, considering the Fisher-Kolmogorov approximation to the radial cell propagation ( $v \approx 2\sqrt{D/\tau}$ ), the normoxic and hypoxic doubling times  $\tau$  (14 and 24 days respectively) can be extrapolated, which are also similar to those used in Rockne et al. (2010). The normoxic oxygen uptake was obtained from a healthy tissue of  $0.2C^{(M)}$  as cell density with oxygen consumption of 15 mmHg/s (Daču et al., 2003). Hypoxic oxygen uptake is several times smaller than the normoxic one as it was observed in U251 glioma cells (Griguer et al., 2008).

Table 1. Typical values of the biological parameters taken for our model equations

Parameter	Value and units	Meaning	Reference	Variation
$C^{(M)}$	$10^6 \text{ cell/cm}^2$	Maximum tumor cell density	Rockne et al. (2010)	No
$O_2^{(S)}$	7 mmHg	Oxygen concentration level switch to hypoxia	Vaupel (2004)	No
$O_2^{(T)}$	2.5 mmHg	Michaelis Menten threshold	Daçu et al. (2003)	No
$O_2^{(D)}$	0.7 mmHg	Critical anoxia level	Brown et al. (2004)	No
$O_2^v$	80 mmHg	Typical oxygen pressure within vessels	Kimura et al. (1996)	No
$\alpha_n$	$7.5 \times 10^{-4} \text{ mmHg c/s}$	Typical normoxic cell oxygen consumption	Daçu et al. (2003)	No
$\alpha_h$	$\alpha_n/5 \text{ mmHg c/s}$	Typical hypoxic cell oxygen consumption	Griguer et al. (2008)	No
$D_{O_2}$	$10^{-5} \text{ cm}^2/\text{s}$	Oxygen diffusion coefficient	Daçu et al. (2003)	No
$\tau_{nh}$	0.15 h	Normoxic to hypoxic phenotype switch time	Jewel et al. (2001)	No
$\tau_{hd}$	7 days	Anoxic death time	Martínez-González et al. (2012)	No
$J_{O_2}$	$10^{-6} \text{ s}^{-1}$	Oxygen flow coefficient	Estimated	No
$\Delta c$	$0.02 C^{(M)}$ cells	Sensitivity vascular threshold	Estimated	No
$D_n$	$5 \times 10^{-10} \text{ cm}^2/\text{s}$	Normoxic and hypoxic diffusion coefficients	Rockne et al. (2010)	10%
$D_h$	$5 \times 10^{-9} \text{ cm}^2/\text{s}$			10%
$\tau_n$	14 days	Normoxic and hypoxic doubling times	Estimated by Fisher-Kolmogorov approx.	10%
$\tau_h$	24 days			10%
$\tau_{hn}$	96 hours	Hypoxic to normoxic phenotype switch time	Semenza (2009) Hsieh (2010)	10%
$C^{(F)}$	$0.5 C^{(M)}$	Critical cell number for fluctuating hypoxia	Ruf et al. (2010)	10%
$C^{(C)}$	$0.7 C^{(M)}$	Critical cell number for chronic hypoxia	Ruf et al. (2010)	5%
$\tau_{hn}$	8-48 hours	Hypoxic to normoxic phenotype switch time under AO therapy	Semenza (2009) Hsieh (2010)	5%
$C^{(F)}$	$0.6\text{-}0.8 C^{(M)}$	Cell number thresholds for fluctuating and chronic hypoxia under AT	Ruf et al. (2010)	5%
$C^{(C)}$	$0.8\text{-}0.99 C^{(M)}$			1%
$RT_{ox}$	0.8	RT surviving fractions in normoxia and hypoxia	Joiner et al. (2009)	5%
$RT_{hyp}$	0.95			5%

## 4.2 Computational details

Henceforth, we consider two possible scenarios: one corresponding to a biopsied but not totally/partially resected tumor, and a second one where the tumor was either partially or totally resected. In both scenarios we will assume that, prior to the application of radiotherapy, or antithrombotic (AT) and antioxidative (AO) therapies, there is a mixture of normoxic cells plus smaller fractions of hypoxic cells and a necrotic core.

In the case of resected tumors initially there will be a small infiltrative tumor remnant located around the surgical border. In that case simulations start two weeks after surgery and all blood vessels are assumed to work correctly, thus  $\chi^C = \chi^F = 1$ . Since the initial cell density is low, there is a good oxygen supply at  $t = 0$  and its redistribution is very fast, we can take  $O_2(x, 0)$  to be roughly uniform in space.

Non-resected tumors will be considered of size  $\approx 1.6$  cm of diameter at diagnosis, with a necrotic core at its center occupying  $\approx 0.8$  cm of diameter. Around the necrotic tissue a high tumor cell density of about 0.6 (in units of  $C^{(M)}$ ) exists and is formed by normoxic and hypoxic cells. This hypercellular region is related to the high-contrast ring which is frequently observed in T1 MRIs (with Gadollinium) of GBMs. In our simulations, the width of this ring is about 4 mm. A very low density of hypoxic cells infiltrating into the healthy tissue (brain parenchima) is also present. Only blood vessels located within the necrotic compartment are considered to be non functional. We will also study smaller tumors for partially resected tumors, of diameter  $\approx 1$  cm after surgery, where the necrotic core is in the center occupying  $\approx 0.2$  cm of diameter and radial tumor infiltration of size  $\approx 0.4$  cm formed by normoxic and hypoxic cells. In that situation we will assume that there are no functional vessels in the center of the tumor.

To solve Eqs. (2.1) and (2.3) numerically we have used a standard finite difference method of second order in time and space with zero boundary conditions along the sides of the computational domain. We have employed large integration domains and cross-checked our results for different domain sizes to avoid spurious edge effects. All the results provided in the following sections are the outcome of sets of ten simulations. Each simulation allows a random static variability (in the range of 1-10%) in the parameters according to the last column in table 1. All variations are constant along time except  $z$  in Eq. 2.5a, which is related to the stochastic temporal variability of oxygen perfusion from the vessels. The error bars shown in the figures correspond to the standard deviations of the results after the full set of simulations corresponding to small variations of the parameters is computed.

## 5. Results

### 5.1 Tumor evolution

We have performed extensive simulations of the model equations (2.1-2.5) with different initial data and for broad parameter ranges of biological significance. A typical result of the tumor density evolution is shown in Fig. 3 for two times (days 72 and 168). In spite of the extensive cytoreduction assumed for the surgery, tumor cells proliferate giving rise to a relapse. The first stages (not shown in the figure) correspond to the proliferation of the normoxic component until a sufficiently high density occurs that leads to vessel instability as described in Sec. 2.3. After 72 days, a number of vessels in the center of the tumor have already collapsed developing anoxic areas as shown in the oxygen distribution (Fig. 3A). As a result, a significant fraction of hypoxic cells start to coexist and compete with the normoxic ones (Fig. 3B). Finally, a necrotic core of about 3 mm in size occupies the center of the tumor (Fig. 3D). Due to the effect of the tumor on the vessel functionality and the differences in the cell uptake coefficients,

there is a significant dispersion of oxygenation levels in regions containing high cell densities.

As the tumor progresses, the area occupied by damaged vessels and necrosis increases with time, and oxygenation decreases due to the destruction of the functional vasculature (Fig. 3E). After 168 days the necrotic core already has a size of 8 mm (Fig. 3H). Necrotic areas are typically surrounded by hypercellular regions generated by the migration of cells from low oxygen areas, resembling the pseudopalisades observed in high-grade gliomas (Brat et al., 2004; Rong et al., 2006).

### 5.2 Targeting vaso-occlusions leads to a small reduction in tumor volume

We have first studied the effect of antithrombotic (AT) therapy improving vessel functionality as described in Sec. 3.1. This therapy reduces invasion speed by keeping cells in their oxic and less motile phenotype but the effect on tumor progression is small. An example is shown in Fig. 4A. Each point represents the average of 10 simulations with mean values and static random variations (Table 1). The error bars indicate the standard deviation of the results of those sets of simulations.

We have used different antithrombotic doses T1, T2, and T3 to delay vessel degradation by the tumor. We suppose that there is a dosis-response effect. The threshold parameters for chronic and fluctuating hypoxia for T3 are  $C^{(C)} = 0.8C^{(M)}$  and  $C^{(F)} = 0.6C^{(M)}$ , for T2:  $C^{(C)} = 0.9C^{(M)}$ ,  $C^{(F)} = 0.7C^{(M)}$  and for T1:  $C^{(C)} = 0.99C^{(M)}$ ,  $C^{(F)} = 0.8C^{(M)}$ . It is clear from Fig. 4 that there are no significant differences with the non-treated tumor volumes until the sixth week; this is the time were the tumor density becomes large enough to impair the vessels. This therapy is able to delay the damage of the vessels but once the new (higher) thresholds are reached no further gains are observed. We have verified this conclusion with a large range of parameters obtaining very similar results. Thus, only minor gains are to be expected from AT therapy unless it is combined with other agents.

### 5.3 Antioxidative therapy has the potential to improve survival substantially

The heterodimer HIF-1 has complex effects on tumor cell biology. On the one hand, the suppression of the HIF-1 $\alpha$  subunit activity severely compromises the ability of tumor cells to undergo anaerobic glycolysis. This reduces the proliferation rate of hypoxic cells and promotes the apoptotic program in cells that are deprived of both oxygen and glucose (Joiner et al., 2009). This is why many therapies have tried to target HIF-1 $\alpha$ , although their effectivity in brain tumors has not been proven yet. In our case we propose antioxidative therapies as a way to normalize the cell response under oxic conditions.

We have used different antioxidant doses O3, O2 and O1, corresponding to a reduction in the normalization times to  $\tau_{hn} = 48, 24$ , and 8 hours respectively. Our simulations encompass a time window of six months for the tumor volume evolution with and without AO therapies. The results are depicted in Fig. 4B. Since the AO therapy promotes the proliferative phenotype, vaso occlusion takes place earlier than in the control case. This leads to the formation of cells actively migrating away from collapsed vessels and the AO therapy does not decrease the tumor volume during the first 4 weeks. However, maintenance of the therapy for longer times produces a significant benefit coming from the essential lessening in the invasion speed. Even assuming a minor effect of the AO therapy (as would be the case with O3) there is a significant tumor volume reduction (12%) after six months. Higher doses/effects of antioxidants (O1 or O2), associated to smaller recovery times, result in substantial tumor volume reductions (up to 40%) (Fig. 4 B). We have used a large range of parameters obtaining similar results that would suggest that a prolonged AO therapy may be beneficial for a large number of patients.

### 5.4 Antithrombotics and antioxidants may have a synergistic effect leading to a substantial tumor

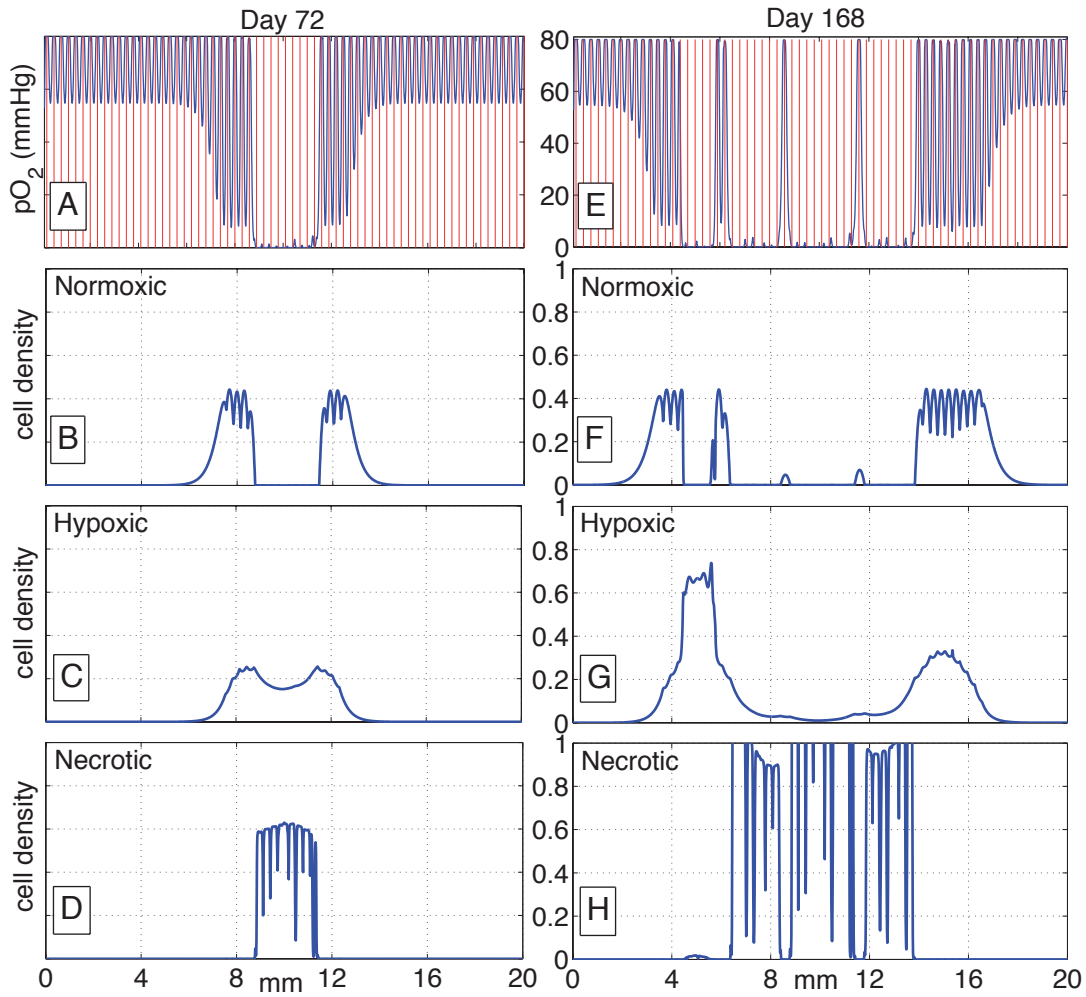


FIG. 3. **Typical evolution of the cell densities and oxygen on a tissue of size 2 cm.** Intermediate distribution (day 72) on the left column and final distribution (day 168) on the right. A and E display tissue oxygenation, B and F the normoxic cell density, C and G the hypoxic cell density and finally, D and H show the necrosis. Red vertical lines at A and E simulate the blood vessels position along the tissue.

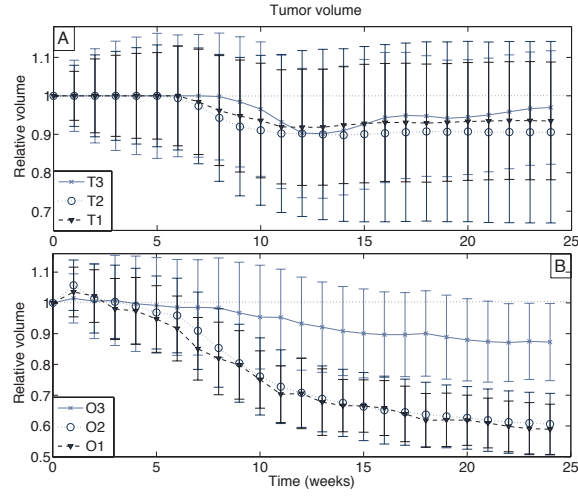


FIG. 4. **Volume of tumors treated with antithrombotics or antioxidants related to non treated tumors.** A: Relative tumor volume for different antithrombotic regimens (T3:  $C^{(C)} = 0.8C^{(M)}$ ,  $C^{(F)} = 0.6C^{(M)}$ , T2:  $C^{(C)} = 0.9C^{(M)}$ ,  $C^{(F)} = 0.7C^{(M)}$ , T1:  $C^{(C)} = 0.99C^{(M)}$ ,  $C^{(F)} = 0.8C^{(M)}$ ). B: Relative tumor volume for different antioxidative regimens (O3:  $\tau_{hm} = 48$  hours O2:  $\tau_{hm} = 24$  hours O1:  $\tau_{hm} = 8$  hours). Dotted lines in A and B are the respective relative volumes for non-treated tumors. Error bars display the standard deviation for the 10 simulations developed for each treatment varying the parameters as indicated in Table 1.

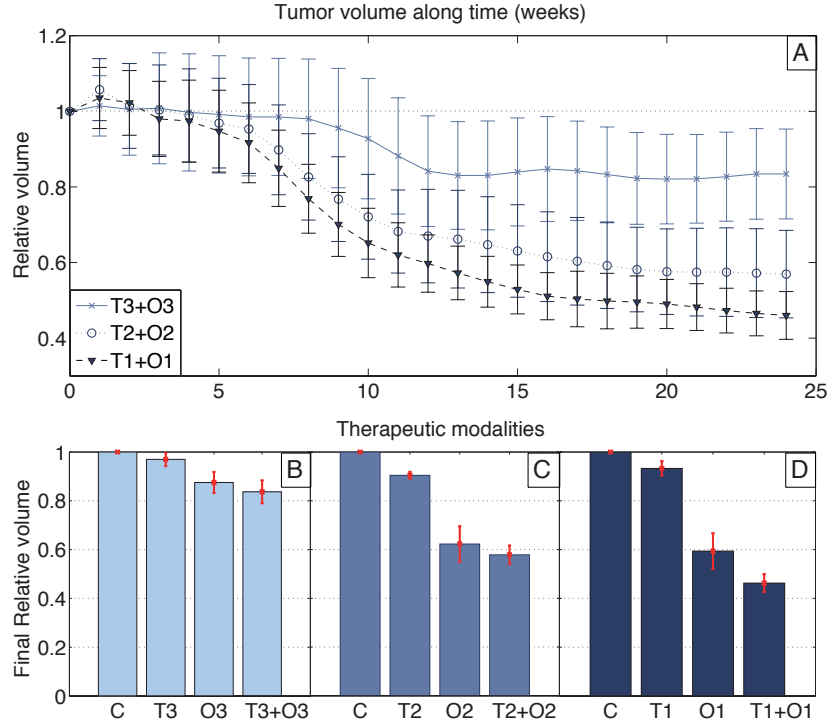


FIG. 5. **Evolution in time of the relative tumor volume under combination therapies with antithrombotics and antioxidants.** A: Tumor volume as a function of time for the three combined treatments relative to the control. The dotted constant line represents the volumes for non treated tumors. Antithrombotic treatments are T3:  $C^{(C)} = 0.8C^{(M)}$ ,  $C^{(F)} = 0.6C^{(M)}$ , T2:  $C^{(C)} = 0.9C^{(M)}$ ,  $C^{(F)} = 0.7C^{(M)}$  and T1:  $C^{(C)} = 0.99C^{(M)}$ ,  $C^{(F)} = 0.8C^{(M)}$ . Antioxidative treatments are O3:  $\tau_{hm} = 48$  hours, O2:  $\tau_{hm} = 24$  hours and O1:  $\tau_{hm} = 8$  hours. B, C, D: Final relative tumor volumes for the different therapeutic modalities considering C as the control (non treated tumor group). Error bars display the standard deviation for the 10 simulations developed for each treatment varying the parameters as indicated in Table 1.

### volume reduction

Having AT and AO together in our mathematical model, has the biological meaning that we are simultaneously targeting the coagulation cascade to delay the invasiveness process and the high levels of free radicals that also have an effect on invasiveness.

Fig. 5 shows the typical outcome of our simulations. We have combined the therapies T1, T2, T3, O1, O2 and O3, as described in Secs. 5.2 and 5.3, to get *in silico* several treatment modalities: T3+O3, T2+O2 and T1+O1, besides the control C, which is the non treated tumor group. The error bars in Fig. 5 display the standard deviation for ten simulations varying the parameters in Table 1, as described previously.

Firstly, Fig. 5A exhibits the tumor volume evolution related to the control for the combined treatments. All treatments show a visible volume reduction from the sixth week. After 24 weeks, the relative tumor volume reduction, as compared to the control, is 0.83, 0.56 and 0.45 for T3+O3, T2+O2 and T1+O1, respectively.

Secondly, Fig. 5 subplots B, C and D show the tumor volumes after six months for each different therapeutic modality. All of them result in a reduction in the final tumor volume after six months of treatment, but in all cases the combination of AT and AO gives the best outcome. In some instances, such as with the most effective therapies T1+O1, a synergistic effect is observed when combining both therapies (see Fig. 5D).

### 5.5 Antithrombotics and antioxidants sensitize the tumor for cytotoxic therapies

An interesting result of our simulations is that the combination of antithrombotics and antioxidants results in a reduction of hypoxic areas and the normalization of cell phenotypes that results in a higher sensitivity to cytotoxic therapies. In what follows we will discuss the action of radiotherapy (RT) together with the AT and AO therapies. As discussed in Sec. 3.3, well oxygenated cells suffer more damage when exposed to radiation. In addition, more aggressive phenotypes, such as those induced by hypoxia, have higher levels of repair enzymes that makes them less sensitive to cytotoxic therapies.

We have run a set of simulations combining RT with AT and AO for tumors of different initial size at diagnosis. We display examples of their evolution, comparing different combination therapies and initial conditions: totally resected tumors after surgery (Fig. 6), partially resected tumors (Fig. 8) and biopsied tumors without an extensive tumor volume reduction (Fig. 7).

A first example of our results is plotted in Fig. 6 where we show the *in silico* predictions for the tumor volume evolution (Fig. 6A), radial tumor velocity (Fig. 6B), for different therapeutic modalities during a period of 58 weeks, together with the final volumes comparing all therapies Fig. 6 C. Following the standard practice for GBM we will assume that RT starts two weeks after surgery and runs for 6 weeks from monday to friday in fractions of 2 Gy. It is clear from Fig. 6A and B that there are no significant volume or growth speed differences between the irradiated tumors until week 12. The effect of RT results in a substantial reduction in tumor volume and tumor growth speed that is still apparent several months after the therapy has finished. It is also obvious that combination therapies of RT with the different agents are always more effective than radiotherapy alone. It is remarkable that the effect of AT+AO is equivalent, after one year, to the effect of RT, though with a much lower toxicity (and long-term effects). At the end of the studied period of 58 weeks, there is a 12% reduction for AT alone and a remarkable 42% decrease with AO alone. The mean final tumor volume for the combination of T1+O1 is similar to the one obtained for tumors receiving only RT; both displaying a reduction of more than 50% when compared to the control group. RT+AT gives rise to about 55% reduction, RT+AO to around 65% and the combination RT+AT+AO exhibits over 70% of tumor volume at week 58th compared to the non-treated tumors.

Our results suggest that a substantial increase of several months in the median overall survival for GBM patients may be obtained by combining RT+AT+AO.

### 5.6 Antithrombotics and antioxidants might be more effective for patients having only a biopsy or subtotal resections

Fig. 7 displays the tumor volume evolution for the different therapeutic modalities during 24 weeks after diagnosis. In this case, the tumor was not resected and its diameter at diagnosis was higher than 1.6 cm. Only vessels located between 20 and 30 mm were considered non functional since almost this space was occupied by dead cells as illustrated in the initial cell density subplot Fig. 7A. Tumor volume evolution is shown in Fig. 7B and evidences how all therapies delay tumor progression almost from the first day, a fact that did not occur for totally resected tumors.



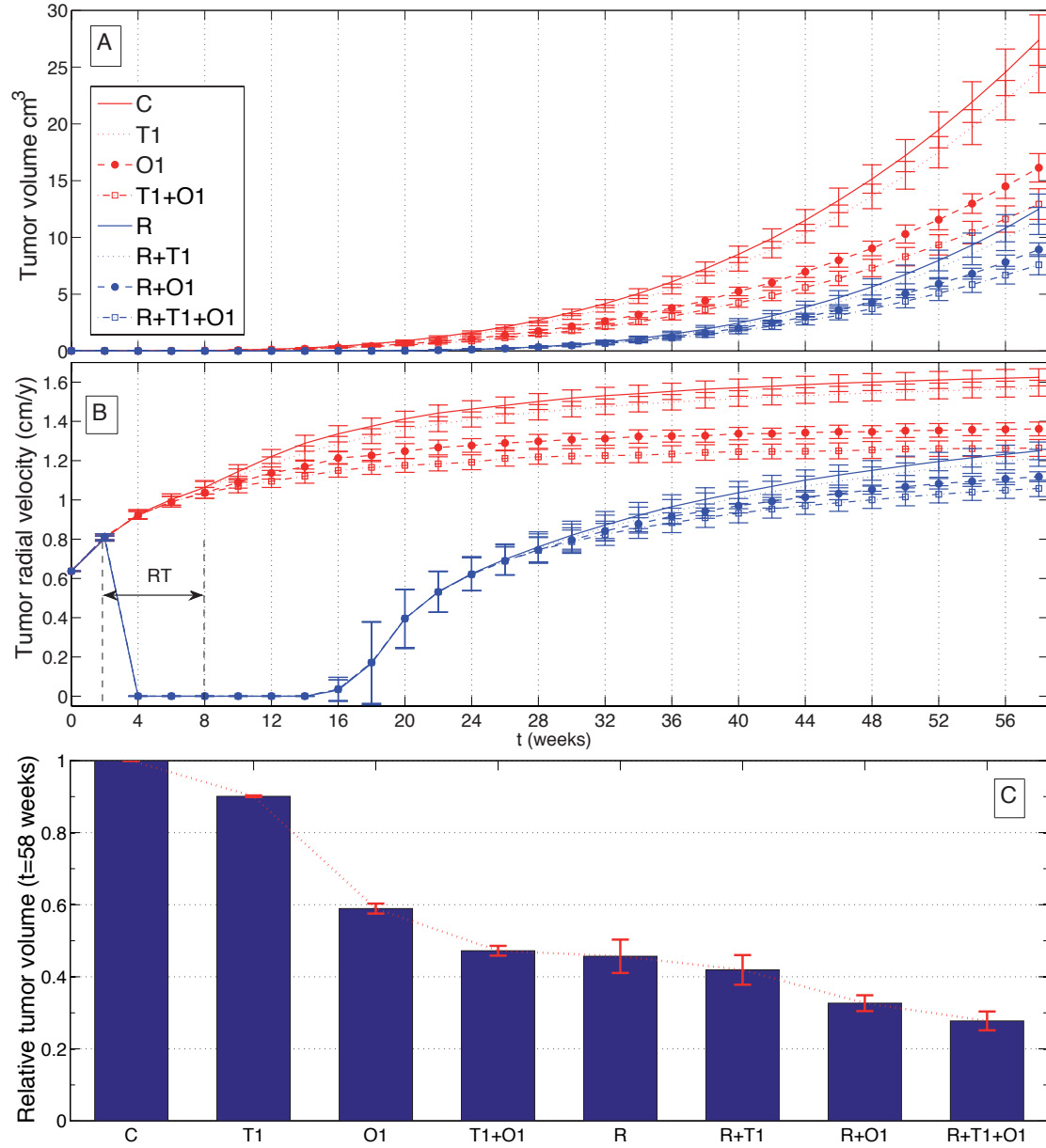


FIG. 6. **Tumor volume and tumor radial velocity for different therapeutic modalities.** Subplots A and B display the tumor volume (cm³) and the tumor radial velocity (cm/y) during 58 weeks, respectively. Each line provides the results for a therapeutic modality: C is the control (non-treated), T1 (antithrombotics):  $C^{(C)} = 0.99C^{(M)}$ ,  $C^{(F)} = 0.8C^{(M)}$ , O1 (antioxidants):  $\tau_{lm} = 8$  hours, T1+O1 (antithrombotics+antioxidants), R (standard radiotherapy with 30 sessions, 2 Gy/session, monday-friday), R+T1 (radiotherapy+antithrombotics), R+O1 (radiotherapy+antioxidants), R+T1+O1 (radiotherapy+antithrombotics+antioxidants). Red curves correspond to non-radiated tumors and blue curves to radiated ones. Subplot C shows the relative final volume for all treatments after 58 weeks. Error bars display the standard deviation for the 3 simulations developed for each treatment varying the parameters as indicated in Table 1.

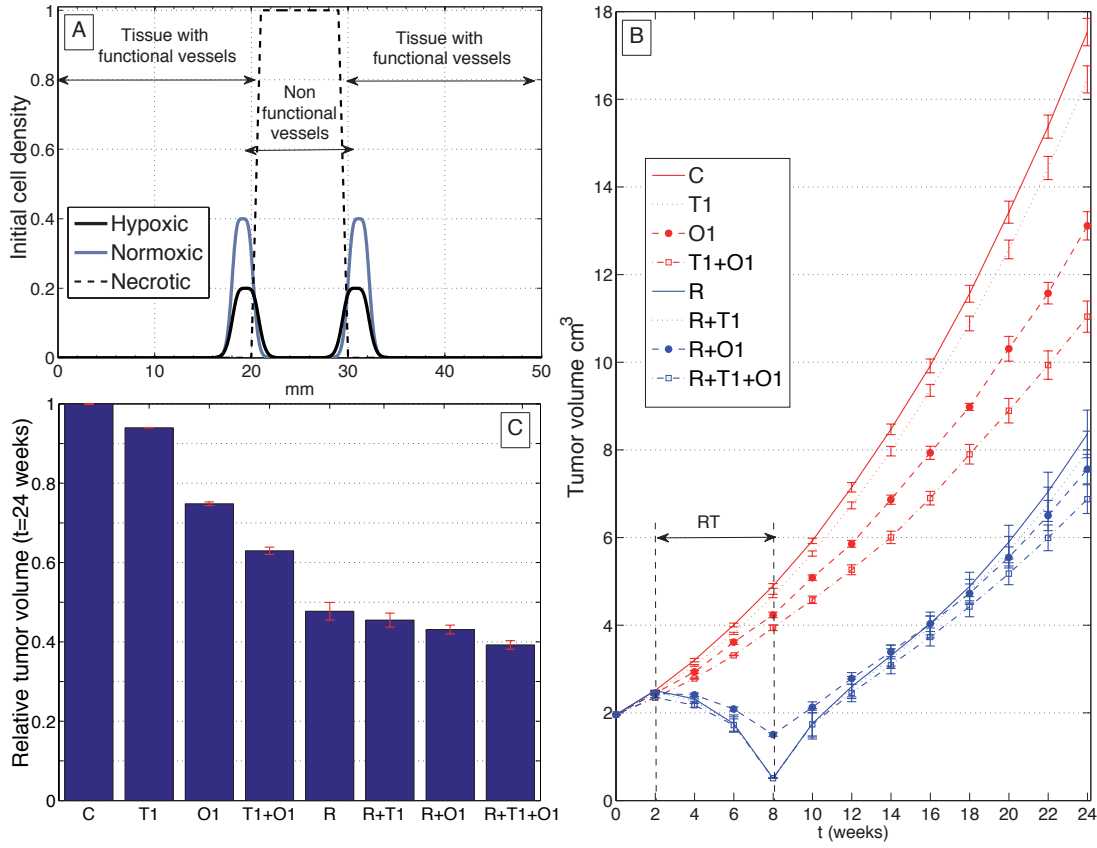


FIG. 7. **Tumor volume evolution for different therapeutic modalities without prior surgery.** Subplot A shows the initial cell density distribution at diagnosis for hypoxic, normoxic and necrotic cells. Initial tumor diameter  $\approx 1.6$  cm, necrotic core  $\approx 0.8$  cm and radial tumor infiltration  $\approx 0.5$  cm. Subplot B displays the tumor volume evolution (cm<sup>3</sup>) during 24 weeks. Each line provides the results for a therapeutic modality: C is the control (non-treated), T1 (antithrombotics):  $C^{(C)} = 0.99C^{(M)}$ ,  $C^{(F)} = 0.8C^{(M)}$ , O1 (antioxidants):  $\tau_{hm} = 8$  hours, T1+O1 (antithrombotics+antioxidants), R (standard radiotherapy with 30 sessions, 2 Gy/session, monday-friday), R+T1 (radiotherapy+antithrombotics), R+O1 (radiotherapy+antioxidants), R+T1+O1 (radiotherapy+antithrombotics+antioxidants). Red curves correspond to non-radiated tumors and blue curves to radiated ones. Subplot C shows the relative final volume for all treatments after 24 weeks. Error bars display the standard deviation for the 3 simulations developed for each treatment varying the parameters as indicated in Table 1.

At the end of the 24 weeks, we find a benefit in the reduction of tumor volume similar to the one obtained from totally resected tumors after 58 weeks of treatment modalities (Fig. 7C). Thus, the group of patients with biopsy or subtotal resection might benefit even more from a combination of AT and AO therapies. In addition, when both AT and AO are used together with radiotherapy a significant advantage is obtained when compared with radiotherapy alone. This gain is more evident for patients having only a biopsy or subtotal resections, than in tumors with small remnants that are expected to be initially well oxygenated.

### 5.7 *Combination of antithrombotics and antioxidants might be more effective than radiotherapy alone*

The last example shown in Fig. 8 displays the tumor volume evolution for the different therapeutic modalities during the first 48 weeks after subtotal resection. In this case, the tumor diameter following surgery was around 1 cm. Initially, the vessels in the center of the tumor were taken to be non functional leading to the formation of a small necrotic core. Hypoxic and normoxic cells, surrounding the necrotic areas, infiltrate into the healthy tissue Fig. 8A. The initial distribution of the partial pressure of oxygen is displayed in Fig. 8B.

After 48 weeks all treated tumors significantly reduced their volume compared to the non treated ones. It is remarkable that radiotherapy implies a 35% reduction versus the 55% reduction observed in Fig. 6C for totally resected tumors. The cause of this fact can be the better initial oxygenation and the absence of necrosis and hypoxic cells in the second case. However, antioxidants and antithrombotics are still as effective as in Fig. 6. In addition, after 48 weeks, the benefit obtained from the combination of AT and AO with radiotherapy is more apparent for these cases (see Fig. 8C).

Although the best result is obtained with a combination of the three proposed therapies, it is important to emphasize the fact that AO alone or AO with AT (without radiation) produced a reduction in tumor volume larger than the one observed under radiotherapy alone (see Fig. 8D).

## 6. Discussion and conclusions

As a consequence of cyclic hypoxia during GBM progression, free radicals are mainly originated from the mitochondrial respiratory chain which regulates the transcription hypoxia-inducible factor HIF-1 $\alpha$  expression. Indeed, hypoxia (particularly via HIF-1 $\alpha$ ) is responsible for metabolic and phenotypic changes which induce invasiveness of GBM cells and initiate coagulation mechanisms that promote tumor growth acceleration.

The antioxidative treatment may result in the inhibition of HIF-1 $\alpha$  leading to a reduction of the tumor invasiveness, delaying progression of GBM in humans. In addition, the increase of free radical could be stabilized by means of an antioxidative therapy, controlling or delaying the vascular degeneration due to the malformations of endothelial cells induced by the HIF-1 $\alpha$  pathway activation. In this way, targeting HIF-1 $\alpha$  can be seen as an attractive approach to complement radiotherapy and chemotherapy, which kill well-oxygenated cells (Joiner et al. (2009); Chen et al. (2011)) and also to inactivate extrinsic HIF-1 $\alpha$  pathways, forcing the tumor to display a lower-grade behavior by reducing invasion and angiogenesis.

Other potential interesting agents for GBM treatment are antithrombotics, such as low molecular weight heparine (LMWH), a low molecular weight heparin that promotes the release of tissue factor pathway inhibitors for preventing venous thromboembolism and with very low toxicities (Planès, 2003). Thus LMWH might be incorporated as a part of GBM treatment to avoid vaso-occlusion phenomena and to delay the neovascularization process associated with this pathology. The results from

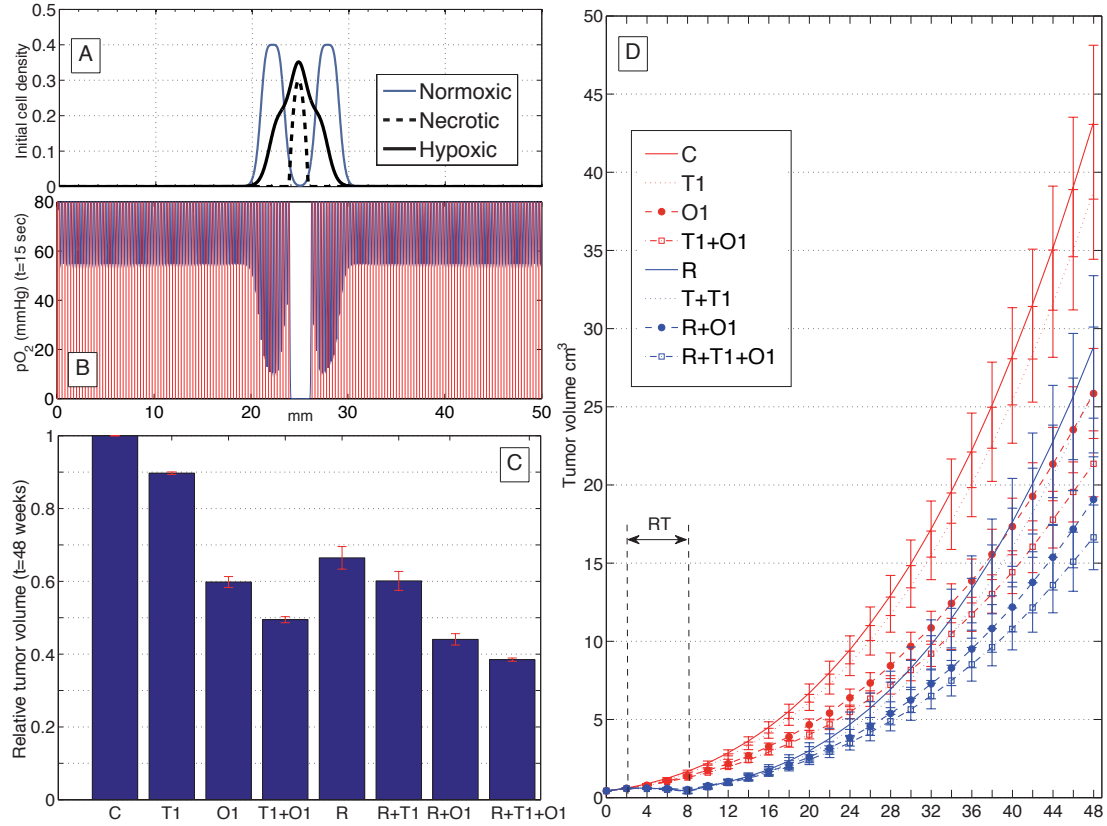


**FIG. 8. Tumor volume evolution for different therapeutic modalities after subtotal resection.** Subplot A shows the initial cell density distribution for hypoxic, normoxic and necrotic cells. Initial tumor diameter  $\approx 1$  cm, necrotic core  $\approx 0.2$  cm and radial tumor infiltration  $\approx 0.4$  cm. B displays the initial distribution of the partial pressure of oxygen. Vertical red lines represent the functional vessels and blue lines the oxygenation along the space. There are no functional vessels at the center of the tumor. Subplot C shows the relative final volume for all treatments after 48 weeks. Subplot D displays the tumor volume evolution ( $cm^3$ ) during 48 weeks. Each line provides the results for a therapeutic modality : C is the control (non-treated), T1 (antithrombotics):  $C^{(C)} = 0.99C^{(M)}$ ,  $C^{(F)} = 0.8C^{(M)}$ , O1 (antioxidants):  $\tau_{hm} = 8$  hours, T1+O1 (antithrombotics+antioxidants), R (standard radiotherapy with 30 sessions, 2 Gy/session, monday-friday), R+T1 (radiotherapy+antithrombotics), R+O1 (radiotherapy+antioxidants), R+T1+O1 (radiotherapy+antithrombotics+antioxidants). Red curves correspond to non-radiated tumors and blue curves to radiated ones. Error bars display the standard deviation for the 3 simulations computed for each treatment varying the parameters as indicated in Table 1.

our model seem to imply that an additional indirect antitumoral effect from thromboprophylaxis might be expected related to the delay of tumor invasion, different from the direct antitumoral effect or the increase in survival and quality of life to be expected from the prevention of the formation of big coagulates. Furthermore, from our simulations shown in Fig. 4A, it follows that an optimum antithrombotic treatment regimen exists (in our case, T2:  $C^{(C)} = 0.9C^{(M)}$ ,  $C^{(F)} = 0.7C^{(M)}$  in comparison with T3 or T1) as evidenced by a U-effect on the relative tumor volume.

In addition, antithrombotic therapy could avoid early tumor-induced vaso occlusions delaying the so-called malignant transformation of low-grade gliomas, were they transition to a high-grade glioma. Consequently, antithrombotic therapy administered to WHO grade II astrocytic and oligodendroglial patients may help to preclude the malignant transformation into secondary GBM associated with the onset of hypoxia once local vascular damage is produced.

Finally, Targeting HIF-1 $\alpha$  and vasculature normalization simultaneously in GBM may have a synergistic effect decreasing tumor invasion and increasing patient overall survival time by changing the tumor microenvironmental behavior from high grade to low grade glioma. In addition, tumor cells have high levels of antioxidative enzymes which contribute to eliminate more efficiently the free radicals produced by alkylating agents such as carmustine (BCNU) or by the radiation. Besides the radiotherapy sensitization obtained with a better tumor oxygenation, the treatment would also reduce the need to activate antioxidative enzymes, rendering the tumor more susceptible to the effect of these agents. Fig. 1 summarizes the possible synergetic effect predicted by our *in silico* model combining antioxidants, antithrombotics and radiotherapy in the GBM treatment.

It is worth to mention the use of anti-angiogenics in the context of the go or grow hypothesis. On the one hand, anti-angiogenic treatments impair tissue oxygenation and promote motile phenotypes to dominate the tumor population and invade faster the adjacent tissue. On the other hand, a pro-vascular therapy may oxygenate the tumor with the risk of producing leaky vessels through which tumor cells can intravasate and form distant foci in the brain parenchyma. This has lead to a long discussion on the potential existence of a window where anti-angiogenic therapies may be useful mainly as a concomitant one. It would be very interesting to develop mathematical models of these phenomena in order to guide the use of these therapies, specially after the recent results clinical trials investigating the combination of antiangiogenic therapies with the standard of care that have shown no impact on overall survival (Herriksson et al., 2013; Wick et al., 2013), though the progression free survival seems to benefit from the use of these drugs.

It is important to remark that stochastic fluctuations in the therapy might affect the tumor dynamics. These changes can be due to stochastic variations of the drug pharmacokinetics as shown by (d'Onofrio and Gandolfi, 2010). However, in this paper we have assumed that drug administration is such that the drugs achieve their therapeutical regimes that is preserved during treatment and constant in each simulation.

Other results from our simulations are that the different treatment modalities proposed suggest a more substantial effect on larger initial tumors than on smaller ones. Thus, the combination of antithrombotics and antioxidants might be more effective for patients having only a biopsy or subtotal resections than for those in which the tumor could be macroscopically resected. In fact, for non resected tumors, a combination of antithrombotics and antioxidants could be more effective than radiotherapy alone probably due to the poor oxygenation and the presence of necrotic and hypoxic areas within the tumor. In addition, this combined therapy could even be more favorable for those patients with high risk of vessel coagulation.

In conclusion, we have developed a biocomputational model of glioblastoma multiforme that incorporates the spatio-temporal interplay among two glioma cell phenotypes corresponding to oxygenated

and hypoxic cells, a necrotic core and the local vasculature whose response evolves with the tumor progression. Our *in silico* approach reveals that the different therapeutic modalities which combine antithrombotics and antioxidants would improve vessel functionality, avoiding vaso-occlusions and reducing oxidative stress and the subsequent hypoxic response. This combined treatment would reduce glioma cell invasion and sensitize glioblastoma to conventional radiotherapy, hopefully increasing patients survival.

### Acknowledgements

This work has been partially supported by grants MTM2012-31073 (Ministerio de Economía y Competitividad, Spain) and the James S. McDonnell Foundation (USA) through the 21st Century Science Initiative in Mathematical & Complex Systems Approaches for Brain Cancer-Pilot Award 220020351.

### References

- BASTIDA, E., ORDINAS, A., ESCOLAR, G., JAMIESON, G.A. (1984) Tissue factor in microvesicles shed from U87MG human glioblastoma cells induces coagulation, platelet aggregation, and thrombogenesis. *Blood* **64**, 177-184.
- BATCHELOR, T.T., BYRNE, T.N. (2006) Supportive care of brain tumor patients. *Hematol. Oncol. Clin. North. Am.* **20**, 1337-1361.
- BERENS, M.E., GIESE, A. (1999) "...those left behind." Biology and oncology of invasive glioma cells. *Neoplasia* **1** 208-219.
- BRAT, D.J., CASTELLANO-SANCHEZ, A.A., HUNTER, S.B., PECOT, M., COHEN, C., HAMMOND, E.H., DEVI, S.N., KAUR, B., VAN MEIR, E.G. (2004) Pseudopalisades in glioblastoma are hypoxic, express extracellular matrix proteases, and are formed by an actively migrating cell population. *Cancer Res.* **64** 920-927.
- BRISTOW, R.G., HILL, R.P. (2008) Hypoxia, DNA repair and genetic instability. *Nature Rev. Cancer* **8** 180-192.
- BROSE, K.M. J., LEE, A.Y.Y. (2008) Cancer-associated thrombosis: prevention and treatment. *Curr. Oncol.* **15** S58-S67.
- BROWN, J., WILSON, W. (2004) Exploiting tumour hypoxia in cancer treatment. *Nature* **4** 437-447.
- COBBS, C.S., WHISENHUNT, T.R., WESEMANN, D.R. , HARKINS, L.E., VAN MEIR, E.G. AND SAMANTA, M. (2003) Inactivation of wild-type p53 protein function by reactive oxygen and nitrogen species in malignant glioma cells. *Cancer Research* **63** 8670-8673.
- CHEN, T.C., WANG, W., GOLDEN, E.B., THOMAS, S., SIVAKUMAR, W., HOFMAN, F.M., LOUIE, S.G., AND SCHNTHAL, A.H. (2011) Green tea epigallocatechin gallate enhances therapeutic efficacy of temozolomide in orthotopic mouse glioblastoma models. *Cancer Lett.* **302** 100108.
- DAÇU, A., TOMA-DAÇU, I., KARLSSON M. (2003) Theoretical simulation of tumour oxygenation and results from acute and chronic hypoxia. *Phys. Med. Biol.* **48** 2829-2842.

- DEBERARDINIS, R.J., MANCUSO, A., DAIKHIN, E., NISSIM, I., YUDKOFF, M., WEHRLI, S., THOMPSON, C.B. (2007) Beyond aerobic glycolysis: Transformed cells can engage in glutamine metabolism that exceeds the requirement for protein and nucleotide synthesis. *Proc. Natl. Acad. Sci. U.S.A.* **104** 19345-19350.
- DEWHIRST, M.W., CAO, Y., MOELLER, B. (2008) Cycling hypoxia and free radicals regulate angiogenesis and radiotherapy response. *Nature Rev. Cancer* **8** 425-437.
- A. D'ONOFRIO AND A. GANDOLFI (2010) Resistance to antitumor chemotherapy due to bounded-noise-induced transitions. *Phys. Rev. E* **82** 061901 [10 pages].
- ELSTNER, A., HOLTkamp, N., VON DEIMLING, A. (2007) Involvement of Hif-1  $\alpha$  in desferrioxamine-induced invasion of glioblastoma cells. *Clin. Exp. Metastasis* **24** 57-66.
- GIESE, A., BJERKVIG, R., BERENS, M.E., WESTPHA, M.L. (2003) Cost of migration: Invasion of malignant gliomas and implications for treatment. *J Clin Oncology* **21** 1624-1636.
- GORIN, F., HARLEY, W., SCHNIER, J., LYETH, B., JUE, T. (2004) Perinecrotic glioma proliferation and metabolic profile within an intracerebral tumor xenograft. *Acta Neuropathol.* **107** 235-244.
- GREEN, D., KWAAN, H.C. (2009) *Coagulation in cancer*, Springer.
- GRIGUER, C.E., OLIVA, C.R., GOBIN, E., MARCORELLES, P., BENOS, D.J., LANCASTER, J.R. JR., GILLESPIE, G.Y. (2008) CD133 is a marker of bioenergetic stress in human glioma. *PloS One* **3** e3655.
- HAMILTON, M.G., HULL, R.D., PINEO, G.F. (1994) Prophylaxis of venous thromboembolism in brain tumor patients. *J. Neurooncol.* **22** 111-126.
- HARTER, P.N., DÜTZMANN, S., DROTT, U., ZACHSKORN, C., HATTINGEN, E., CAPPER, D., GESSLER, F., SENFT, C., SEIFERT, V., PLATE, K.H., KÖGEL, D., AND MITTELBRONN, M. (2013) Anti-tissue factor (TF9-10H10) treatment reduces tumor cell invasiveness in a novel migratory glioma model. *Neuropathology* DOI:10.1111/neup.12018.
- HATZIKIROU, H., BASANTA, D., SIMON, M., SCHALLER, K., DEUTSCH, A. (2010) 'Go or Grow': the key to the emergence of invasion in tumour progression. *Math. Med. Biol.* **29** 49-65.
- HENRIKSSON R, BOTTOMLEY A, MASON W, SARAN F, WICK W, NISHIKAWA R, CLOUGHESY TF, CARPENTIER AF, HOANG-XUAN K, KAVAN P, CERNEA D, BRANDES AA, HILTON M, ABAJO-GUIJARRO AA, RAVELO A, CHINOT OL (2013) Progression-free survival (PFS) and health-related quality of life (HRQoL) in AVAglio, a phase III study of bevacizumab (Bv), temozolomide (T), and radiotherapy (RT) in newly diagnosed glioblastoma (GBM). *J. Clin. Oncol.* **31**, Suppl; abstr 2005.
- HSIEH, C-H., LEE, C-H., LIANG, J-A., YU, C-Y., SHYU, W-C. (2010) Cycling hypoxia increases U87 glioma cell radioresistance via ROS induced higher and long-term HIF-1 signal transduction activity. *Oncology Reports* **2** 1629-1636.
- HUBBI, M.E., KSHITIZ, GILKES, D.M., REY, S., WONG, C.C., LUO, W., KIM, D-H., DANG, C.V., LEVCHENKO, A., SEMENZA, G.L. (2013) A nontranscriptional role for HIF-1  $\alpha$  as a direct inhibitor of DNA replication. *Science Signaling* **6** ra10.

- JENKINS, E.O., SCHIFF, D., MACKMAN, N., KEY, N.S. (2010) Venous thromboembolism in malignant gliomas. *J. Thromb. Haemost.* **8** 221-227.
- JEWELL, U.R., KVIETIKOVA, I., SCHEID, A., BAUER, C., WENGER, R.H., GASSMANN M. (2001) Induction of Hif-1 $\alpha$  in response to hypoxia is instantaneous. *FASEB J.* **15** 1312-1314.
- JOINER, M., AND VAN DER KOGEL, A. (2009) *Basic Clinical Radiobiology*,
- KALLIOMAKI, T. M., MCCALLUM, G., WELLS, P. G., HILL, R. P. (2009) Progression and metastasis in a transgenic mouse breast cancer model: Effects of exposure to in vivo hypoxia. *Cancer Lett.* **282** 98-108.
- KELLY, C., SMALLBONE, K., BRADY, M. (2008) Tumour glycolysis: The many faces of HIF. *J. Theor. Biol.* **254** 508-513.
- KEUNEN, O., JOHANSSON, M., OUDIN, A., SANZEY, M., RAHIM, S.A., FACK, F., THORSEN, F., TAXT, T., BARTOS, M., JIRIK, R., MILETIC, H., WANG, J., STIEBER, D., STUHR, L., MOEN, I., RYGH, C.B., BJERKVIG, R., NICLOU, S.P. (2011) Anti-VEGF treatment reduces blood supply and increases tumor cell invasion in glioblastoma. *Proc. Natl. Acad. Sci. U.S.A.* **108** 3749-3754
- KHORANA, A.A., FRANCIS, C.W. (2008) Cancer associated thrombosis: New findings in translational science, prevention, and treatment. *Informa Healthcare U.S.A., Inc.*
- KIMURA, H., BRAUN, R.D., ONG, E.T., HSU, R., SECOMB, T.W., PAPAHA DJOPOULOS, D., HONG, K., AND DEWHIRST, M.W. (1996) Fluctuations in red cell flux in tumor microvessels can lead to transient hypoxia and reoxygenation in tumor parenchyma. *Cancer Res.* **56** 5522-5528.
- KOVACIC, P., OSUNA, J.A. (2001) Mechanism of carcinogenesis: focus on oxidative stress and electron transfer. *Curr. Med. Chem.* **8** 773-796.
- LOUIS, D.N., OHGAKI, H., WIESTLER, O.D., CAVENEE, W.K. (2007) World Health Organization Classification of Tumours of the Central Nervous System, 4th ed., *Renouf Publishing Co. Ltd., Geneva*.
- MARTÍNEZ-GONZÁLEZ A., CALVO G.F., PÉREZ ROMASANTA L.A., PÉREZ-GARCÍA V.M. (2012) Hypoxic cell waves around necrotic cores in glioblastoma: A biomathematical model and its therapeutic implications. *Bull. Math. Biol.* **74** 2875-2896.
- ONISHI, M., ICHIKAWA, T., KUROZUMI, K., DATE, I. (2011) Angiogenesis and invasion in glioma. *Brain Tumor Pathol.* **28** 13-24.
- PAINTER, K.J., HILLEN, T. (2013) Mathematical modelling of glioma growth: The use of Diffusion Tensor Imaging (DTI) data to predict the anisotropic pathways of cancer invasion. *J. Theor. Biol.* **323** 25-39.
- PLANÈS, A. (2003) Review of bemiparin sodium—a new second-generation low molecular weight heparin and its applications in venous thromboembolism. *Expert Opin. Pharmacother.* **4** 1551-1561.
- POGUE, B.W., PAULSEN, K.D., OHARA, J.A., WILMOT, C.M., SWARTZ, H.M. (2001) Estimation of oxygen distribution in RIF-1 tumors by diffusion model-based interpretation of pimonidazole hypoxia and Eppendorf measurements. *Radiat. Res.* **155** 15-25.



- POWATHIL, G.G., GORDON, K.E., HILL, L.A., CHAPLAIN, M.A.J. (2012) Modelling the effects of cell-cycle heterogeneity on the response of a solid tumour to chemotherapy: Biological insights from a hybrid multiscale cellular automaton model. *J. Theor. Biol.* **308** 1-19.
- ROCKNE, R., ROCKHILL, J.K., MRUGALA, M., SPENCE, A.M., KALET, I., HENDRICKSON, K., LAI, A., CLOUGHESY, T., ALVORD, JR., E.C., SWANSON, K.R. (2010) Predicting the efficacy of radiotherapy in individual glioblastoma patients in vivo: a mathematical modeling approach. *Phys. Med. Biol.* **55** 3271-3285.
- RONG, Y., POST, D.E., PIEPER, R.O., DURDEN, D.L., VAN MEIR, E.G., BRAT, D.J. (2005) PTEN and hypoxia regulate tissue factor expression and plasma coagulation by glioblastoma. *Cancer Res.* **65** 1406-1413.
- RONG, Y., DURDEN, D.L., VAN MEIR, E.G., AND BRAT, D.J. (2006) 'Pseudopalisading' necrosis in glioblastoma: A familiar morphologic feature that links vascular pathology, hypoxia, and angiogenesis. *J. Neuropathol. Exp. Neurol.* **65** 529-539.
- RUF, W., YOKOTA, N., SCHAFFNER, F. (2010) Tissue factor in cancer progression and angiogenesis. *Thrombosis Res.* **125** S36-S38.
- DOS SANTOS, C., KARAKY, R., RENOIR, D., HAMMA-KOURBALI, Y., ALBANESE, P., GOBBO, E., GRISCELLI, F., OPOLON, P., DALLE, S., PERRICAUDET, M., COURTY, J., DELBÉ, J. (2010) Antitumorigenic effects of a mutant of the heparin affinity regulatory peptide on the U87 MG glioblastoma cell line. *Int. J. Cancer* **127** 1038-1051.
- SCHNEIDER, T., MAWRIN, C., SCHERLACH, C., SKALEJ, M., AND FIRSCHING, R. (2012) Gliomas in adults. *Dtsch. Arztebl. Int.* **107** 799-808.
- SCHUMACKER, P. T. (2006) Reactive oxygen species in cancer cells: Live by the sword, die by the sword. *Cancer Cell* **10** 175-176.
- SEMENZA G.L. (2009) Regulation of cancer cell metabolism by hypoxia-inducible factor 1. *Seminars in Cancer Biology* **19** 12-16.
- SEMENZA G.L. (2012) Hypoxia-inducible factors in physiology and medicine. *Cell* **148** 399-408.
- SIMANEK, R., VORMITTAG, R., HASSLER, M., ROESSLER, K., SCHWARZ, M., ZIELINSKI, C., PABINGER, I., MAROSI, C. (2007) Venous thromboembolism and survival in patients with high-grade glioma. *Neuro-Oncology* **9** 89-95.
- STREIFF, M.B., SEGAL, J., GROSSMAN, S.A., KICKLER, T.S., WEIR, E.G. (2004) ABO blood group is a potent risk factor for venous thromboembolism in patients with malignant gliomas. *Cancer* **100** 1717-1723.
- SVENSSON, K.J., KUCHARZEWSKA, P., CHRISTIANSON, H.C., SKÖLD, S., LÖFSTEDT, T., JOHANSSON, M.C., MÖRGELIN, M., BENGZON, J., RUF, W., BELTING, M. (2011) Hypoxia triggers a proangiogenic pathway involving cancer cell microvesicles and PAR-2-mediated heparin-binding EGF signaling in endothelial cells. *Proc. Nat. Acad. Sci.* **108** 13147-13152.
- TENNANT, D.A., DURÁN, R. V., GOTTLIEB, E. (2010) Targeting metabolic transformation for cancer therapy. *Nature Rev. Cancer* **10** 267-277.

- VAN MEIR, E.G., HADJIPANAYIS, C.G., NORDEN, A.D., SHU, H.-K., WEN, P.Y., OLSON, J.J. (2010) Exciting new advances in neuro-oncology: The avenue to a cure for malignant glioma. *CA Cancer J. Clin.* **60** 166-193.
- VAUPEL, P. (2004) The role of hypoxia-induced factors in tumor progression. *The Oncologist* **9** 10-17.
- VAUPEL, P., THEWS, O., HOECKEL, M. (2001) Treatment resistance of solid tumors: Role of hypoxia and anemia. *Med. Oncol.* **18** 243-259.
- WICK W, CLOUGHESY TF, NISHIKAWA R, MASON W, SARAN F, HENRIKSSON R, HILTON M, KERLOEGUEN Y, CHINOT OL (2013) Tumor response based on adapted Macdonald criteria and assessment of pseudoprogression (PsPD) in the phase III AVAglio trial of bevacizumab (Bv) plus temozolomide (T) plus radiotherapy (RT) in newly diagnosed glioblastoma (GBM). *J. clin Oncol* **31**, suppl; abstr 2002.
- WILSON, W.R., HAY, M.P. (2011) Targeting hypoxia in cancer therapy. *Nature Rev. Cancer* **11** 393-410.
- YOUNG, A., CHAPMAN, O., CONNOR, C., POOLE, C., ROSE, P., KAKKAR, A.K. (2012) Thrombosis and cancer. *Nature Rev. Clin. Oncol.* **9** 437-449.